

Interturn Short Fault Diagnosis in a PMSM by Voltage and Current Residual Analysis with the Faulty Winding Model

Seokbae Moon *Student member, IEEE*, Hyeyun Jeong, Hojin Lee, and Sang Woo Kim, *Member, IEEE*

Abstract—As interturn short fault (ISF) in a permanent-magnet synchronous machine (PMSM) degrades its energy efficiency and may cause other problems, accurate fault diagnosis for the PMSMs is necessary. In this paper, we present a method that uses voltage and current residual components to diagnose the phase and the severity of the ISF in PMSMs. A faulty-winding model (FWM) is introduced to analyze the fault; the model describes a relationship between the voltage decrease of the faulty winding to the characteristics of the fault such as a fault resistance and a fault turn ratio. Based on the model, we suggest a fault index (FI) that shows the severity of the ISF. As the ISF induces residual components to both voltage and current, the proposed method utilized those components with the FWM. A least squares (LS) method is used to estimate the FI and to diagnose the ISF of PMSMs. Experimental results demonstrate that the proposed method diagnose the ISF effectively.

Index Terms—interturn short fault, PMSM, model, fault diagnosis, fault index, faulty winding model.

NOMENCLATURE

R_f	Resistance that models insulation degradation
μ_p	Short turn ratio to total turns in one phase
μ_w	Short turn ratio to total turns in a faulty winding
V_f	Voltage drop of shorted turns
i_f	Circulating current in shorted turns
ψ_{PM}	Flux linkages of permanent magnets (PMs)
θ	Electrical angular positions
R_s	Resistance of stator coils
L	Self-inductance of stator coils
M	Mutual-inductance of stator coils
L_{sm}	Static component of L
L_{sl}	Leakage component of L
V_{abc}	Stator voltage vector
V_a	a -phase voltage
i_{abc}	Stator current vector
i_a	a -phase current
N	Number of windings per phase
L_f	Fault inductance component
γ	Coupling factor of windings
$V_{a,h}$	a -phase voltage in healthy machine

Manuscript received Nov 21, 2016; revised Feb 8, 2017; revised April 26, 2017; This research was supported by the MSIP(Ministry of Science, ICT and Future Planning), Korea, under the ICT Consilience Creative Program (IITP-R0346-16-1007) supervised by the IITP(Institute for Information and communications Technology Promotion).

Authors are with the Department of Electrical Engineering, POSTECH (Pohang University of Science and Technology), 77 Cheongam-Ro, Pohang 37673, Republic of Korea e-mail: (msbworld, jhy90, suvvs, and swkim@postech.edu).

L_{an} N th winding in phase a

$V_{a,fw}$ Faulty winding's voltage when phase a has the ISF

I. INTRODUCTION

PERMANENT magnet synchronous machines (PMSMs) are widely used in many industrial applications owing to their various advantages. PMSMs have higher efficiencies, higher power-to-volume ratios and more precise torque control than induction machines [1]. These features make them attractive candidates especially for electric and hybrid vehicles [2]. With the rising demand for the PMSMs in numerous industrial areas, there is an increasing possibility of unexpected system failures. Faults in PMSMs may result in plant breakdown, economic losses, and even human casualties. To prevent such catastrophies, fault diagnosis for PMSMs are necessary and has studied in recent years [3], [4].

The types of faults that can occur in PMSMs are classified into two groups: One is a mechanical fault including bearing faults [5], and static/dynamic eccentricity faults [6]. The other is an electrical fault such as electrically short or open circuit faults [7], and a demagnetization fault [8]. In PMSMs, an interturn short fault (ISF) is the most common among the electrical faults [9] and also the most critical fault because a high circulating current flows in the shorted circuit [10]. The ISF occurs when the insulation degraded between adjacent coils of the stator windings [11]. A degraded patch of insulation is usually modeled with fault characteristics, which are R_f and μ_p . The patch causes a local reversal in the magnetic field, induces i_f , and generates excessive heat that may increase the severity of the fault [12].

Many studies have been presented to diagnose the ISF. Motor current signature analysis (MCSA), usually using frequency analysis such as using the Fourier transform [13], or the wavelet transform [14] can be easily applied to diagnose the fault. But these techniques usually cannot distinguish the severity of the fault accurately. Several model-based analyses have been tried to diagnose the ISF, e.g., zero-sequence method suggested a fault index based on the extra voltage components induced by the fault [15] and a Kalman filter with fully shorted PMSM model tried to detect μ_p [16]. However, both approaches were only applicable to very severe fault conditions with fully shorted condition and may not applicable in more weaker fault conditions. Another approach that monitors q -axis current harmonics could detect weaker fault than conventional methods [17], but this method needs

a steady-state condition and it is hard to diagnose the fault accurately because the harmonic components are much smaller than the fundamental component.

This paper proposes a simple method for early diagnosis of the ISF by considering voltage and current residual analysis based on a faulty-winding model (FWM) for PMSMs. We analyzed conventional ISF models and fault phenomenon given by finite element analysis (FEA) tool in section II. Based on the analysis, we developed the FWM that shows a relationship between the fault characteristics and the voltage drop of the winding with the ISF in section III. The FI was derived from the FWM in section IV and is estimated using the least squares (LS) method to voltage and current residual components in Section V. The faulty phase was detected by comparing the FIs of the three voltage residual components (VRC) from the three phase voltages. The severity of the fault was determined by the value of the FI. In case of the VRC is so small that cannot separated with the noise, we adopted an additional step which utilizes a q -axis current residual component (CRC). As the proposed method is aimed to diagnose the ISF when the fault is much weaker than conventional studies, we call it ‘early stages’. Section VI shows an experiments results which were conducted on an interior-type PMSM (IPMSM) that suffered from the ISF; experiments considered several operating conditions, including different operating speeds, constant load, and varying load. We also varied R_f and μ_p to implement various conditions from weak faults to severe faults. Experimental results demonstrate that the proposed method estimate the value of the FI well and diagnose the ISF effectively.

II. SIMULATION OF THE PMSM WITH THE ISF

Several tools can be used to analyze magneto-electric characteristics. FEA allows coupling between nonlinear magnetic and electric circuits, and considers flux and current variations to simulate and analyze machine characteristics [18]. We used Ansys Maxwell to implement and analyze the IPMSM, and Simplorer to operate the machines with a proper control algorithm. We used a maximum torque per ampere (MTPA) to control the IPMSM.

PMSMs are operated under various conditions, such as varying load torque and varying current with different speeds. Stator currents and PM produce flux, which orient the magnetic field in the IPMSM. We analyzed the effect of the ISF by monitoring the flux orientation and the flux density distribution given by the FEA.

We implemented the ISF in the IPMSMs and imposed variation by choosing different values of R_f and μ_w . We have 12 sets of fault conditions with combination of $R_f = [0.5, 0.2, 0.1, 0.05 \Omega]$ and $\mu_w = [0.2, 0.4, 0.6]$ in the FEA environment. With our notation, $\mu_w = 0.2$ means that 20 percent of one winding is shorted; because each phase includes six windings, this describes that $\mu_p = \frac{\mu_w}{6} = 0.033$ with other researchers’ notations [15], [16].

Several studies have analyzed the effect of the ISF. It causes a high circulating current that affects the insulation of the coil adjacent to the shorted circuit and increases the

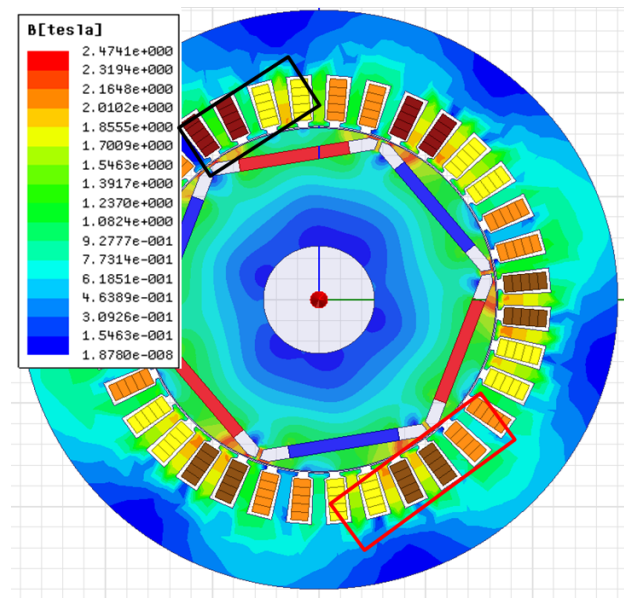


Fig. 1. Flux density distribution given by Maxwell, an FEA simulation of the IPMSM. The ISF in the upper part (a black rectangle) shows less flux than the normal part (a red rectangle). Flux density increases from blue to red.

severity of the fault [12]. Very severe ISF can result rapidly in the demagnetization fault [19]. Flux variation caused by the shorted circuit has been analyzed and a model was introduced [11]. Fig. 1 shows that the ISF causes a flux decrease, because i_f induces a reverse magnetic field at the shorted circuit. The area with the fault (a black rectangle in the Fig. 1) had lower flux density than the normal winding (a red rectangle in the Fig. 1). As you can see in the FEA simulation result, this phenomenon affects not only the faulty part, but also the whole winding that includes the fault. It is because the flux passes through the winding and the normal part shares the flux with the faulty part (Fig. 2). The relatively low flux of the faulty winding means that the magnitude of the voltage drop is smaller at the faulty winding than at the normal winding. For this reason, we analyzed the winding with the fault and developed the FWM, which is introduced in the next section.

III. ISF MODEL AND FWM FOR PMSMS

A. Model of the PMSM with the ISF

An electrical model of a PMSM that is wye-connected winding structure, in the stationary (abc) frame, is given as [20]

$$[V_{abc}] = R_s [I_{abc}] + \frac{d}{dt} ([L_s][I_{abc}] + [\psi_{PM,abc}]) \quad (1)$$

If the ISF occurs in the phase a of the PMSM, the structure of the PMSM is described as using an additional circuit as shown in Fig. 3 and fault terms are added to (1) as:

$$[V_{abc}] = R_s [I_{abc}] + \frac{d}{dt} ([L_s][I_{abc}] + [\psi_{PM,abc}]) - \frac{\mu_w}{N} (R_s [A_1] i_f) - \frac{\mu_w}{N} \frac{d}{dt} ([L M M]^t i_f) \quad (2)$$

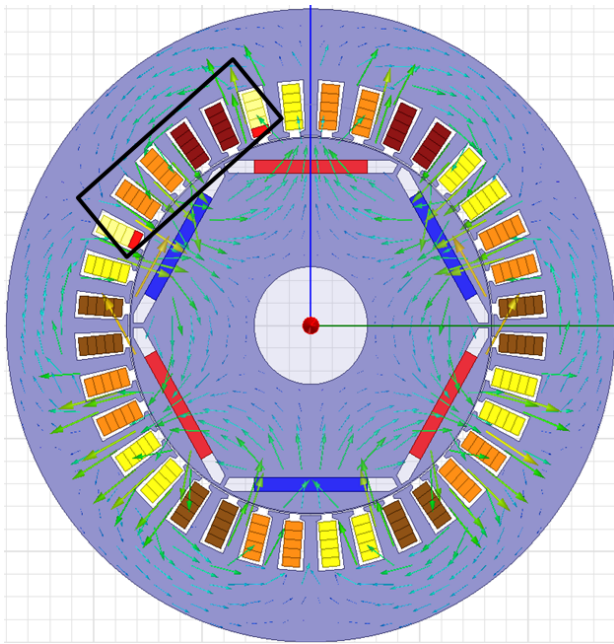


Fig. 2. Field orientation of the IPMSM given by Maxwell. A black rectangle region of faulty winding; small two red rectangles in the black square: interturn short circuits. The faulty winding shares flux (green arrows) with the faulty part.

where $[V_{abc}] = [V_a \ V_b \ V_c]^t$, $[I_{abc}] = [i_a \ i_b \ i_c]^t$, $[L_s] = \begin{bmatrix} L & M & M \\ M & L & M \\ M & M & L \end{bmatrix}$, $[\psi_{PM,abc}] = \psi_{PM} \begin{bmatrix} \cos\theta \\ \cos(\theta - \frac{2\pi}{3}) \\ \cos(\theta + \frac{2\pi}{3}) \end{bmatrix}$. The added component of (2) indicates the faulty part where $[A_1] = [100]^t$. The equation shows an influence of the fault current on phase voltages. However, this equation cannot fully represent the ISF phenomenon because the equation does not consider the multi-pole structure of the PMSMs, which usually have series or parallel windings.

A model that is based on the conventional one above, but that focuses on the faulty part describes a relationship between fault voltages and the fault current at the shorted circuit is also introduced [11]. But according to the FEA simulation result, the fault current affects not only the faulty part, but also the normal part in the same winding. This phenomenon occurs because the normal part shares the flux with the faulty part and the magnitude of the voltage drop in the winding with the fault gets smaller, as mentioned in the previous section (Fig. 2). Therefore, we developed another representation to describe those effect and the characteristics of the faulty winding, especially the decrease of the voltage drop.

B. Model of the Faulty Winding with the ISF

We adopted an analysis from [11] because it considered series windings. Moreover, it took account an interaction between the faulty part and the normal part of the whole winding. This makes the ISF model from [11] to describe the fault phenomenon more accurate than conventional representations. However their model was too complicate and difficult to apply on detecting the fault so that J. Lee introduces more simple model based on the [11] and it is given as follows [21]:

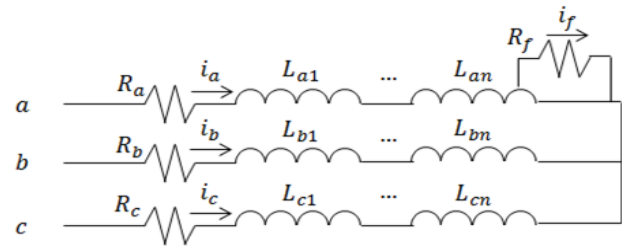


Fig. 3. Stator coil structure of series, wye-connected PMSM with the ISF in phase a.

$$V_a = \left(\frac{NR_f}{\mu_w} + \left(1 - \frac{\mu}{N}\right) R_s \right) i_f + \frac{d}{dt} (\mu_w L_f i_f) \quad (3)$$

where

$$L_f = \left(\frac{1}{1 - \gamma} - \frac{1}{N} \right) L_{sm} + \left(1 - \frac{1}{N}\right) L_{sl} \quad (4)$$

is defined in [21], and γ is defined in [11]. L_{sm} and L_{sl} are represented as $L = L_{sm} + L_{sl}$. These equations are much simpler, and easier to understand than the model from [11]. However, the new model is still difficult to apply to fault diagnosis because it has a differential term. This is why we developed the FWM.

We rewrite the first row of (2) as

$$V_a = V_{a,h} - \frac{\mu_w}{N} R_s i_f - \frac{\mu_w}{N} \frac{d}{dt} (L i_f) \quad (5)$$

where $V_{a,h}$ is the same as the first row of (1). If γ is ignorable (i.e., $\gamma \approx 0$), then (3) can be modified with (5) because $L_f = \frac{N-1}{N} L$ by definition. According to our FEA simulation result, γ has a value less than 0.012, so it is ignorable and we can modify our analysis as follows:

$$V_a - \frac{N-1}{N} V_{a,h} = \left(\frac{R_f}{\mu_w} + (1 - \mu_w) \frac{1}{N} R_s \right) i_f \quad (6)$$

The left side of (6) represents the voltage drop of the faulty winding (L_{an} in Fig. 3) and the right side is composed of the fault resistance, the fault ratio and the fault current. This equation demonstrates that the voltage drop of the faulty winding depends only on the fault characteristics, and is independent of operation conditions such as rotational speed and load torque. The term in the right side of (6) shows the relationship between the fault current and the voltage of the faulty winding, and therefore can be represented as $R_{f\text{fault impedance}}$.

IV. FAULT INDEX FOR THE ISF

A. Ideal Fault Indices for the ISF

Two major parameters affect the severity of the ISF. One is the degraded insulation, which is represented as R_f and that directly indicates the severity of the fault because it is inverse proportional to the magnitude of the fault current; Small R_f induces a large fault current in the shorted circuit. The other parameter is μ , which also affects the characteristics

of the fault such as the magnitude and the phase of the fault current. These values are independent of the stator currents, the rotational speed, and other operation conditions; hence, they are ideal indices for the severity of the ISF.

Unfortunately, the fault model is not sufficient to determine these two parameters uniquely and separately. It is difficult to measure directly the fault voltage V_f and the fault current i_f in real applications. This makes hard to diagnose the severity of the fault accurately. Conventional methods tried to determine the severity of the fault with a specific FI but they diagnosed the fault with very severe conditions [15] or to estimate the fault turn ratio μ_p by assuming that $R_f = 0$ [16].

B. Proposed Fault Index for the ISF

Because R_f and μ_w cannot be estimated separately, we suggest a new FI to diagnose the ISF. The proposed FI enables estimation of the severity of the fault.

Equation (5) can be rewritten as

$$i_f = \left(\frac{R_f}{\mu_w} + (1 - \mu_w) \frac{1}{N} R_s \right)^{-1} \left(V_a - \frac{N-1}{N} V_{a,h} \right) \quad (7)$$

Substituting (7) for i_f in the first row of (2) yields

$$\begin{aligned} V_a - V_{a,h} &= -\frac{\mu_w}{N} R_s i_f - \frac{\mu_w}{N} \frac{d}{dt} (L i_f) \\ &= -\frac{\mu_w}{N} \frac{1}{R_{fault\ impedance}} (R_s V_{a,fw} + \frac{d}{dt} (L V_{a,fw})) \end{aligned} \quad (8)$$

where $V_{a,fw} = V_a - \frac{N-1}{N} V_{a,h}$, which has the same value as the faulty winding's voltage. Here, we propose a new FI for the ISF as follows:

$$FI = \frac{\mu_w}{R_{fault\ impedance}} = \left(\frac{R_f}{\mu_w^2} + \left(\frac{1}{\mu_w} - 1 \right) \frac{1}{N} R_s \right)^{-1} \quad (9)$$

The value of the proposed FI is determined by only R_f and μ_w unless R_s and N do not change. In (8), terms $-\frac{\mu_w}{N} R_s i_f - \frac{\mu_w}{N} \frac{d}{dt} (L i_f)$ are declared as a VRC because those terms are induced by the ISF and could be get from difference between the measured voltage V_a and calculated value from $V_{a,h}$. When the motor is operated without the ISF, $FI = 0$; as the severity of the fault increases, either R_f decreases or μ_w increase; in either case, FI increases.

V. SCHEME TO DIAGNOSE THE ISF

The diagnosis of the ISF is consisted of several processes (Fig. 4). In the first stage, we calculate the VRC of three phase voltages, for example, in case of phase a , $V_a - V_{a,h}$. With the result from the previous step, we detect the phase with the fault among the three phases (abc) by comparing FIs. FIs are estimated through the LS method with the VRC of each phase. However, when the VRC is too small to estimate the FI accurately, there is an additional step which uses the CRC of a q -axis current instead of VRC to get the severity of the fault. In other words, we have two options with the fault diagnosis; the first is using the VRC alone; the second is using the VRC and the CRC together.

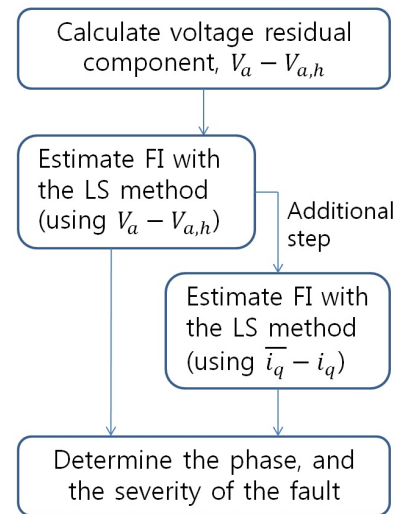


Fig. 4. Flowchart of the proposed ISF diagnosis.

A. Diagnosis of the ISF with the VRC

The fault model of the PMSM that has the ISF in phase a is described as (2). If the fault occurs in phase b , (2) changes as

$$\begin{aligned} [V_{abc}] &= R_s [I_{abc}] + \frac{d}{dt} ([L_s] [I_{abc}] + [\psi_{PM,abc}]) \\ &\quad - \frac{\mu_w}{N} (R_s [A_2] i_f) - \frac{\mu_w}{N} \frac{d}{dt} ([M \ L \ M]^t i_f) \end{aligned} \quad (10)$$

where $[A_2] = [0 \ 1 \ 0]^t$; if the fault occurs in phase c , then

$$\begin{aligned} [V_{abc}] &= R_s [I_{abc}] + \frac{d}{dt} ([L_s] [I_{abc}] + [\psi_{PM,abc}]) \\ &\quad - \frac{\mu_w}{N} (R_s [A_3] i_f) - \frac{\mu_w}{N} \frac{d}{dt} ([M \ M \ L]^t i_f) \end{aligned} \quad (11)$$

where $[A_3] = [0 \ 0 \ 1]^t$. (9) and (10) can be rewritten as (8) by substituting (7) of i_f :

$$\begin{aligned} V_b - V_{b,h} &= -\frac{\mu_w}{N} R_s i_f - \frac{\mu_w}{N} \frac{d}{dt} (L i_f) \\ &= -\frac{\mu_w}{N} \frac{1}{R_{fault\ impedance}} (R_s V_{b,fw} + \frac{d}{dt} (L V_{b,fw})) \end{aligned} \quad (12)$$

$$\begin{aligned} V_c - V_{c,h} &= -\frac{\mu_w}{N} R_s i_f - \frac{\mu_w}{N} \frac{d}{dt} (L i_f) \\ &= -\frac{\mu_w}{N} \frac{1}{R_{fault\ impedance}} (R_s V_{c,fw} + \frac{d}{dt} (L V_{c,fw})) \end{aligned} \quad (13)$$

where $V_{b,fw} = V_b - \frac{N-1}{N} V_{b,h}$ (when the ISF occurs in phase b) and $V_{c,fw} = V_c - \frac{N-1}{N} V_{c,h}$ (when the ISF occurs in phase c). $V_{b,h}$ is a b -phase voltage in the absence of the ISF, (the second row of (1)), and $V_{c,h}$ is a c -phase voltage in the absence of the ISF (the third row of (1)).

To estimate the proposed FI from (8), (12), and (13), we used the LS method. The LS method is one of the most popular

methods for parameter identification [8]. Using this method, we can obtain the optimal solution for a moving-average model system with additive white Gaussian noise [22].

If parameters such as L , M , R_s and ψ_{PM} are known exactly in (8), then (9) can be estimated using the LS method. The rearranged equation of the FI for application of the LS method is

$$FI = -N(V_a - V_{a,h})(R_s V_{a,fw} + \frac{d}{dt}(LV_{a,fw}))^{-1} \quad (14)$$

FI of each phase could be calculated in the same way. Because we assumed the ISF with only one phase, and because the fault phase has bigger VRC than other phases, a comparison of FIs from equations (8), (12), and (13) identifies the phase that has the fault. If the highest FI among those three exceeds the threshold, the motor is diagnosed as having the ISF.

B. Diagnosis of the ISF with the CRC: an Additional Step

FI indicates the severity of the ISF. Use of the LS method with the VRC works well when the VRC is quite large. However in several fault conditions, the magnitude of the VRC is too small to diagnose the ISF accurately (Fig. 5); the peak amplitude of the voltage residual component is about 5 V and it is largely affected by experimental noise. In this case, it is difficult to diagnose the fault using the VRC.

We adopted an additional step to solve this problem. PMSMs are usually operated with current control such as MTPA, so using CRC guarantee more accurate result than using VRC. If the VRC with the highest FI; the VRC of the phase with the fault is less than 10 percent of the phase voltage without the ISF, we use the CRC to diagnose the ISF. In other case; the VRC is large enough and above 10 percent of the phase voltage, we just use the result from the diagnosis with the VRC. We choose the current component of a synchronous frame, especially the q -axis current because its magnitude is usually much bigger than that of a d -axis current in the PMSM.

With Park's transform, the electrical model of the PMSM is written as

$$V_d = R_s i_d + \frac{d}{dt}(L_d i_d) - w_e L_q i_q \quad (15)$$

$$V_q = R_s i_q + \frac{d}{dt}(L_q i_q) + w_e L_d i_d + w_e \psi_{PM} \quad (16)$$

If the PMSM has the ISF, Park's transform changes the ISF model (2) to

$$V_d = R_s i_d + \frac{d}{dt}(L_d i_d) - w_e L_q i_q - \frac{2}{3} R_s \mu_w i_f \cos\theta - \frac{2}{3} w_e L_q \mu_w i_f \sin\theta - \frac{2}{3} L_q \mu_w \frac{d}{dt}(i_f) \cos\theta + \frac{2}{3} w_e L_d \mu_w i_f \sin\theta \quad (17)$$

$$V_q = R_s i_q + \frac{d}{dt}(L_q i_q) + w_e L_d i_d + w_e \psi_{PM} + \frac{2}{3} R_s \mu_w i_f \sin\theta - \frac{2}{3} w_e L_d \mu_w i_f \cos\theta + \frac{2}{3} L_q \mu_w \frac{d}{dt}(i_f) \sin\theta + \frac{2}{3} w_e L_q \mu_w i_f \cos\theta \quad (18)$$

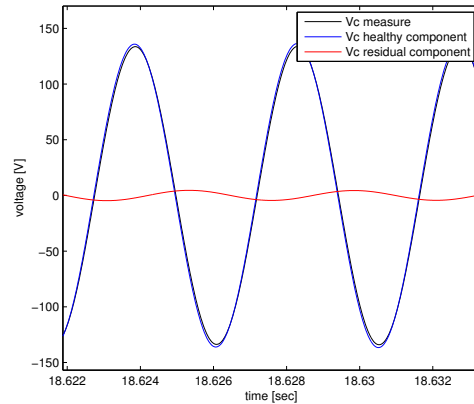


Fig. 5. Voltage residual component (VRC) of the phase c due to the ISF, given by experimental result ($R_f=1.1 \Omega$, $\mu=0.5$)

We can rewrite (17) and (18) by substituting with the following current equations.

$$i'_d = i_d - \frac{2}{3} \mu_w i_f \cos\theta \quad (19)$$

$$i'_q = i_q + \frac{2}{3} \mu_w i_f \sin\theta \quad (20)$$

then (17) and (18) changes to:

$$V'_d = R_s i'_d + \frac{d}{dt}(L_d i'_d) - w_e L_q i'_q \quad (21)$$

$$V'_q = R_s i'_q + \frac{d}{dt}(L_q i'_q) + w_e L_d i'_d + w_e \psi_{PM} \quad (22)$$

where V'_d and V'_q are the measured voltages of the d -axis and the q -axis respectively, including the fault terms, and i'_d and i'_q are the measured currents of the d -axis and the q -axis, respectively. In (19), i_d is the d -axis current and in (20), i_q is the q -axis current in a healthy condition, respectively; in the absence of the ISF and it could be calculated from a healthy PMSM model (1). According to the equations from (15) to (22), the ISF induces current residual components to both d -axis and q -axis current of the PMSM. We utilized q -axis current residual component and FI can be estimated using (20) by substituting (7) for i_f :

$$i'_q = i_q + \frac{2}{3} \left(\frac{R_f}{\mu_w^2} + \left(\frac{1}{\mu_w} - 1 \right) \frac{1}{N} R_s \right)^{-1} \times \left(V_a - \frac{N-1}{N} V_{a,h} \right) \sin\theta \quad (23)$$

$$FI = \frac{3}{2} (i'_q - i_q) \left(V_a - \frac{N-1}{N} V_{a,h} \right)^{-1} (\sin\theta)^{-1} \quad (24)$$

Applying the LS method to (24) yields the value of the FI.

TABLE I
SPECIFICATIONS OF THE IPMSM USED IN THE EXPERIMENTS

Parameters	
Pole pairs	3
Rated current	8.4 A
Rated torque	4.7 Nm
d -axis inductance	2.836 mH
q -axis inductance	5.999 mH
Stator resistance	0.43 Ω
Back EMF constant	36 V/kr/min

VI. EXPERIMENTAL RESULTS

A. Experimental Arrangement

Experimental results were obtained from a 2.2-kW Fmain22-BBFB1 IPMSM manufactured by HIGEN and its specification is given in Table I. The IPMSM has 6 poles, 36 slots and 6 series, wye-connected, and concentrating type windings per phase. The IPMSM was driven by a SV022iG5A-2 inverter manufactured by LSIS. We chose MTPA to operate the IPMSM in the experiments. The IPMSM was coupled with a HD-715 hysteresis dynamometer, a dynamo machine to measure a torque and to give a load torque at the same time (Fig. 6). We used sensors with a 100-kHz sampling rate to acquire voltage and current signals.

The experiments were conducted on healthy and faulty motors. The IPMSM was given the ISF by connecting a resistor between stator winding turns of the last winding in phase c (Fig. 6). We varied the severity of the fault by choosing different resistors R_f and different turn ratio μ_w ; thirteen cases were used (Table II). We used both μ_w and μ_p and it is different with conventional researches, so the short turn ratio is represented with μ_p in the table. Case 0 refers to a healthy motor and cases 1-12 refer to faulty motors. Although case 1 refers to the weakest fault and cause 12 refers to the severest fault, the numbers do not generally correspond to severity. The magnitude of the fault current is 2 A at case 1 and increases according to the severity of the fault, reaches almost 50 A at case 12.

We chose two different experimental sets of nonstationary conditions to verify the proposed algorithm. The first set maintained 3000 rpm and the second set maintained 4500 rpm; to identify how operating speed and currents affect the ISF, both sets were given a varying load torque. The torque loaded to the motor was increased step-by-step from 0 to 4.5 Nm to operate the IPMSMs. The fault current was not affected by increasing torque and current, but was determined by only the fault characteristics (Fig. 7).

Data from 0 to 10 s were not used for algorithm verification, because this period contains the operation starting signal and lacks any significant information. As we varied the torque, the current varied from 0 to 8.2 A during the period from 10 to 45 s. When we apply the proposed algorithm to the experimental data, we performed a pre-process which filters only the fundamental signals and get rid of the harmonics.

B. Result of the Proposed Diagnosis Scheme

The proposed fault diagnosis method was applied to the experimental data and diagnosed whether the IPMSM had a

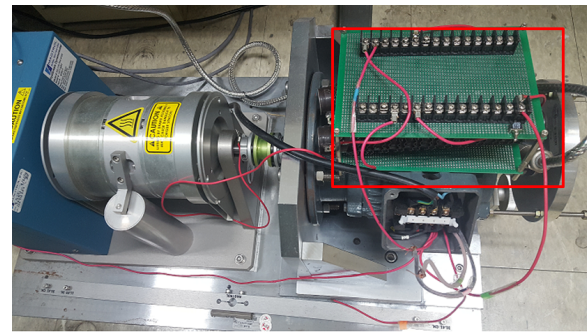


Fig. 6. Experimental setup: The IPMSM with the interturn short fault (ISF) tap (a red square), coupled with the dynamo machine.

TABLE II
VARIOUS FAULT CONDITIONS

Case	1	2	3	4	5	6
R_f [Ω]	1.11	0.63	0.35	0.21	1.11	0.63
μ_p	0.04	0.04	0.04	0.04	0.08	0.08

Case	7	8	9	10	11	12
R_f [Ω]	0.35	0.21	1.11	0.63	0.35	0.21
μ_p	0.08	0.08	0.12	0.12	0.12	0.12

fault or not. First, we verified the FWM under various fault conditions (Fig. 8). The experimental results demonstrate that the proposed FWM describes the fault effect well. As the severity of the fault increase, the flux in the faulty winding become less than those in the healthy winding. This phenomenon results in a decrease of the voltage drop in the faulty winding as mentioned before, and the experimental results show this effect well.

As the FWM is proven to describe the fault phenomenon well, we applied our proposed diagnosis method to experimental results to diagnose the ISF in the IPMSM. As mentioned previously, we calculate the VRC in the first stage. And based on the magnitude of the VRC, the algorithm uses either only the VRC or the VRC and the CRC together. In our experimental environment, the threshold of using CRC or not; the VRC of the phase with the fault is less than 10 percent of the phase voltage happens between the case 6 and 7.

Our proposed method worked well with various fault conditions. All diagnoses indicated that the ISF occur in phase c (Fig. 9). The severity of the fault was also diagnosed (Fig. 10, 11). There is a yellow line in both figures which represents the threshold to distinguish the normal and the faulty motors. Experimental results demonstrate that the proposed fault diagnosis method is not affected by operating speeds (Fig. 10). However, the proposed method was affected by the load torque (Fig. 11). Moreover, in case of the severest fault (the case 12), it shows a poor result. During the fault diagnosis, we assumed the parameters of the IPMSM are not affected by the ISF in the early stages. Based on the assumption, we used normal parameters to calculate $V_{c,h}$ in (13) and estimating the FI. However, the ISF affects the flux distribution of the IPMSM and different flux distribution can cause the change of the parameters of the motors [8]. And the parameters vary according to the severity of the ISF [23]. This difference

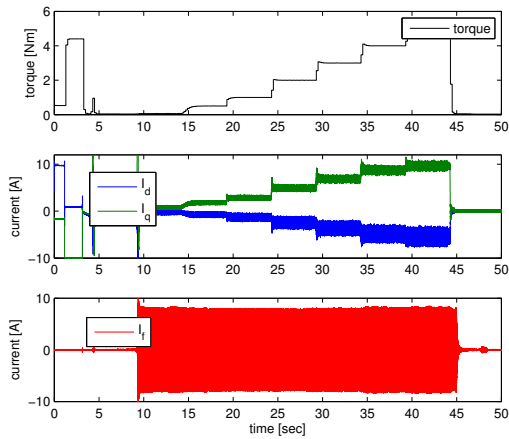


Fig. 7. Torque, dq -axis and fault current of IPMSM operation (case 3)

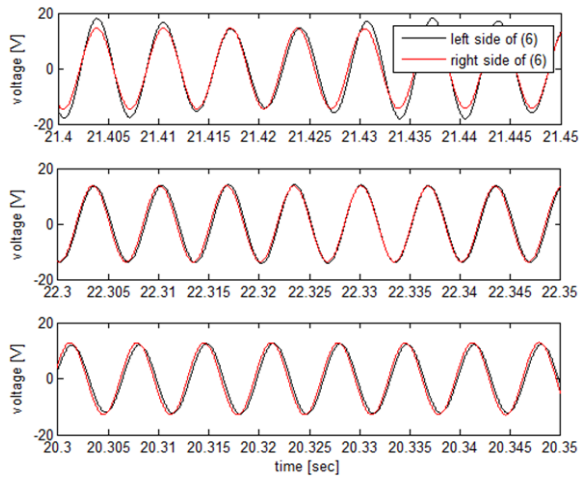


Fig. 8. Experimental results to verify the faulty winding model (FWM) with various fault conditions (fault cases 1, 5, and 9)

caused a large error with the severest case.

The proposed algorithm was applied to the different load torque conditions at 4500 rpm; one is a no load condition (almost 0 Nm, 9 to 14 s) and the other is a full load condition (4.5 Nm, 39 to 44 s). The proposed method was affected by the magnitude of the stator current and showed variation of FI (Fig. 11). The proposed method was affected by the magnitude of the stator current and showed bigger errors in case 1 to 6. Although the proposed method shows a variation to the load torque, we can diagnose the fault with all the other cases because they showed an increasing tendency according to the increasing current. Based on the result, we can diagnose and distinguish the severity of the fault with a measurement of the load torque. If the machine is used in a specific environment with constant torque, the proposed algorithm can separate various fault conditions.

C. Comparing with conventional studies

There have been many studies tried diagnosis of the ISF. However, Fourier transform analysis [13] could not diagnose

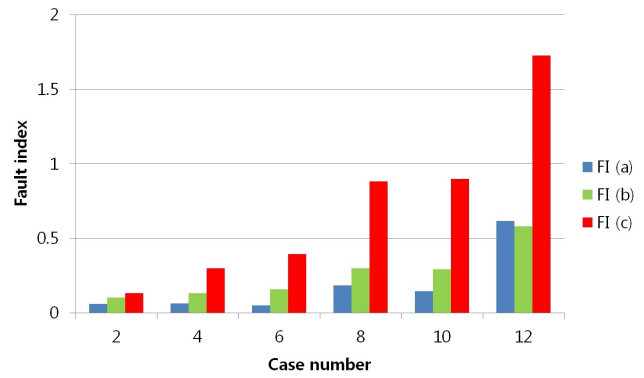


Fig. 9. Experimental result of detecting faulty phase with various fault conditions (at 4500 rpm)

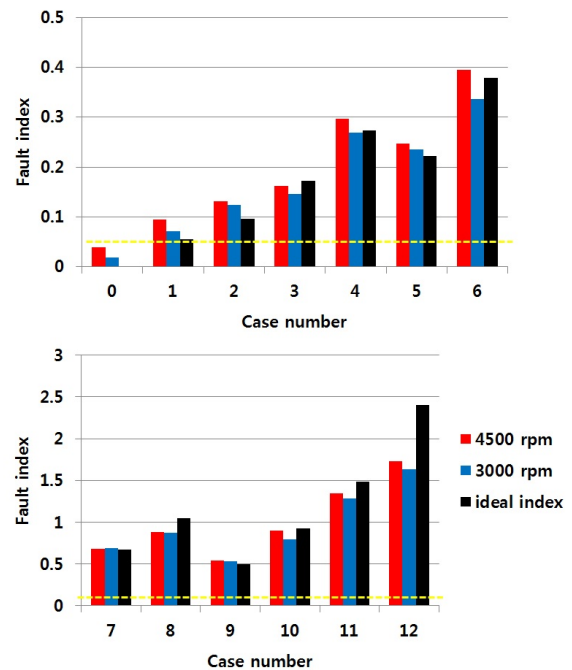


Fig. 10. Experimental results for the diagnosis of the ISF at 2 Nm load torque, with different operating speeds: normal (Case 0) and fault cases 1-12

the ISF in the early stages and also showed poor performance to distinguish a severe fault from a weak fault (Fig. 12).

In case of model-based approaches, most of those techniques diagnosed the ISF in very severe fault conditions. B. Aubert *et al* assumed a fully shorted condition and gave a fault indicator with the application of Kalman filter [16]. Because they assumed a fully shorted condition and expanded fault model, those indicators do not work at all in our experimental data so it was difficult to compare it with the proposed method. In case of the zero-sequence voltage component (ZSVC) analysis, the method also assumed a fully shorted condition and they need a specific equipment named 'balanced register' [15]. As we did not use the balanced register during the experiment, it may give a different result. According to the analysis, the ZSVC is increased as the ISF gets severe. They suggested a fault indicator which is utilizing

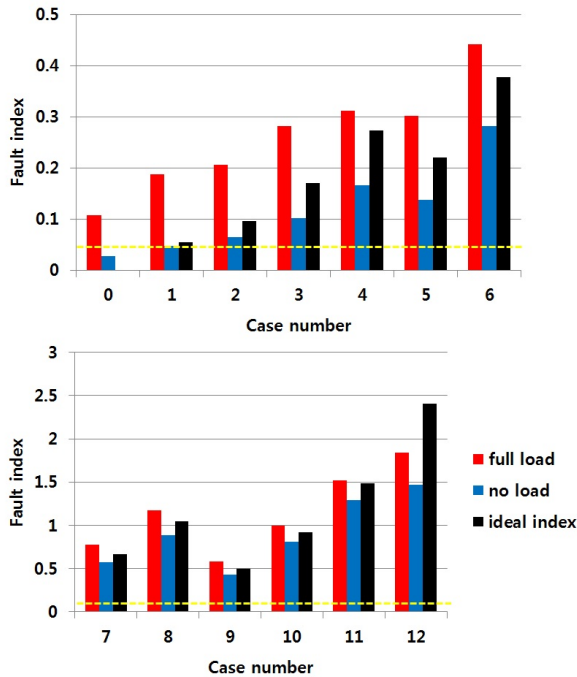


Fig. 11. Experimental results for the diagnosis of the ISF at 3000 rpm, with different load torque: normal (Case 0) and fault cases 1-12

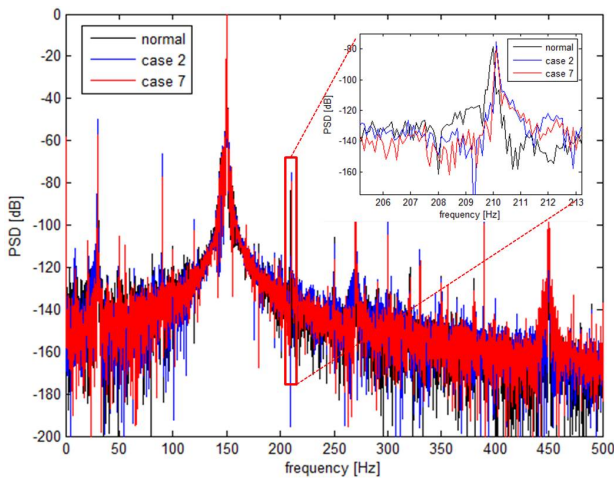


Fig. 12. Frequency analysis of the PMSM with various short conditions

the magnitude of the ZSVC. However, the ZSVC did not show any increasing tendency in our experimental data (Fig. 13) and it means that the ZSVC analysis cannot diagnose the ISF in the early stages.

We also tried a method of monitoring a q -axis current harmonics [17]. The method used a fault indicator of $I_F = h_{q2}/h_{2n}$ where h_{q2} represents the second-order harmonics of the q -axis current with the ISF and h_{2n} represents the magnitude of the second-order harmonic contained in the q -axis under the normal nonfault condition. As h_{2n} was calculated with an interpolation technique and used as a constant, we calculated only h_{q2} in several faulty conditions here and they are given in Table III. Their fault indicator generally shows a good result of distinguishing the fault but there is a possibility

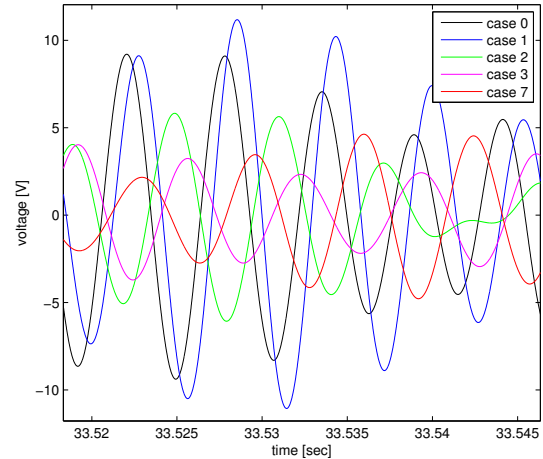


Fig. 13. ZSVC of the PMSM with various short conditions

TABLE III
RESULTS OF MONITORING q -AXIS CURRENT HARMONICS

rpm torque [Nm]	3000 0	3000 2	3000 4	4500 0	4500 2	4500 4
case 2	0.063	0.201	0.287	0.078	0.130	0.183
case 4	0.175	0.318	0.407	0.153	0.215	0.269
case 7	0.424	0.615	0.722	0.477	0.534	0.616

of misdiagnosis since it is largely affected by not only the torque but also the operating speed. On the other hand, our method proposed in this paper is only affected by the torque and works generally well in the early stages as shown in the previous section.

VII. CONCLUSION

This paper proposes an algorithm that utilizes voltage and current residual components based on the FWM to diagnose the ISF of the PMSM. Many studies have attempted to diagnose the ISF, but most of them did not consider the winding that has the fault, and usually focused on very severe conditions. Because it can result in an increase in severity, or cause other faults such as a demagnetization fault, the ISF must be diagnosed in its early stages.

We diagnosed the ISF with the following steps; First, we developed a FWM that describes the voltage drop of the winding that has the ISF. As it showed satisfactory results with experimental data, we proposed a FI based on the FWM. Applying the LS method to estimate the FI with the VRC, we can determine which phase has the fault. We could estimate the severity of the fault under various fault conditions, including early stages of the fault considering either the VRC or the VRC and the CRC together. The proposed method is affected by the magnitude of the stator current, but it is not affected by the operating speed. Considering the magnitude of the load torque, the proposed method can diagnose the fault effectively and it is applicable to the PMSMs in EVs since those machines are operated under various operating speed and torque conditions. Further, the proposed method can diagnose the ISF in the early stages while conventional studies do not work at all.

REFERENCES

- [1] Kwang Hee Nam, "AC Motor Control and Electric Vehicle Applications," CRC press, 2010.
- [2] A. Emadi, Y. J. Lee, and K. Rajashekara, "Power electronics and motor drives in electric, hybrid electric, and plug-in hybrid electric vehicles," *IEEE Trans. Ind. Electron.*, vol. 55, no. 6, pp. 2237-2245, June 2008.
- [3] A. C. Malloy, R. F. Martinez-Botas, and M. Lamperth, "Measurement of magnet losses in a surface mounted permanent magnet synchronous machine," *IEEE Trans. Energy Convers.*, vol. 30, no. 1, pp. 323-330, Mar 2015.
- [4] J. Hang, S. Ding, J. Zhang, M. Cheng, W. Chen, and Q. Wang, "Detection of inter-turn short-circuit fault for PMSM with simple fault indicator," *IEEE Trans. Energy Convers.*, vol. 31, no. 4, pp. 1697-1699, Dec 2016.
- [5] B. Zhang, C. Sconyers, C. Byington, R. Patrick, M. E. Orchard, and G. Vachtsevanos "A probabilistic fault detection approach: Application to bearing fault detection," *IEEE Trans. Ind. Electron.*, vol. 58, no. 5, pp. 2011-2018, May 2011.
- [6] F. R. Alam, B. Rezaeacalam, and J. Faiz, "Unbalanced magnetic force analysis in eccentric surface permanent-magnet motors using an improved conformal mapping method" *IEEE Trans. Energy Convers.*, vol. PP, no. 99, pp.1-1, Nov 2016.
- [7] G. Choi, and T. M. Jahns, "Investigation of key factors influencing the response of permanent magnet synchronous machines to three-phase symmetrical short-circuit faults," *IEEE Trans. Energy Convers.*, vol. 31, no. 4, pp.1488-1497, Dec 2016.
- [8] S. Moon, J. Lee, H. Jeong, and S. W. Kim, "Demagnetization Fault Diagnosis of a PMSM Based on Structure Analysis of Motor Inductance," *IEEE Trans. Ind. Electron.*, vol. 63, no. 6, pp. 3795-3803, June 2016.
- [9] M. A. Awadallah, M. M. Morcos, S. Gopalakrishnan, and T. W. Nehl, "Detection of stator short circuits in VSI-fed brushless dc motors using wavelet transforms," *IEEE Trans. Energy Convers.*, vol. 21, no. 1, pp. 1-8, Mar 2006.
- [10] S. M. A. Cruz and A. J. M. Cardoso, "Multiple reference frames theory: A new method for the diagnosis of stator faults in three-phase induction motors," *IEEE Trans. Energy Convers.*, vol. 20, no. 3, pp. 611-619, Sept 2005.
- [11] BG. Gu, JH. Choi, and IS Jung, "Development and Analysis of Interturn Short Fault Model of PMSMs with Series and Parallel Winding Connections," *IEEE Trans. Power Electron.*, vol. 29, no. 4, pp. 2016-2026, April 2014.
- [12] B. Vaseghi, B. Nahid-Mobarakh, N. Takorabet, and F. Meibody-Tabar, "Inductance identification and study of PM motor with winding turn short circuit fault," *IEEE Trans. Magnetics.*, vol. 47, no. 5, pp. 978-981, May 2011.
- [13] J. Penman, H. G. Sedding, B. A. Lloyd, and W. T. Fink, "Detection and location of interturn short circuits in the stator windings of operating motors," *IEEE Trans. Energy Convers.*, vol. 9, no. 4, pp. 652-658, Dec 1994.
- [14] J. Seshadrinath, B. Singh, and B. K. Panigrahi, "Investigation of Vibration Signatures for multiple fault diagnosis in variable frequency drives using complex wavelets," *IEEE trans. Power Electron.*, vol. 29, no. 2, pp. 936-945, Feb 2014.
- [15] J. Hang, J. Zhang, M. Cheong and J. Huang, "Online Interturn Fault Diagnosis of Permanent Magnet Synchronous Machine Using Zero-Sequence Components," *IEEE Trans. Power Electron.*, vol. 30, no. 12, pp. 6731-3741, Dec 2015.
- [16] B. Aubert, J. Regnier, S. Caux, and D. Alejo, "Kalman-Filter-Based Indicator for Online Interturn Short Circuits Detection in Permanent-Magnet Synchronous Generators," *IEEE Trans. Ind. Electron.*, vol. 62, no. 3, pp. 1921-1930, Mar 2015.
- [17] KH. Kim, Simple online fault detecting scheme for short-circuited turn in a PMSM through current harmonic monitoring," *IEEE Trans. Ind. Electron.*, vol. 58, no. 6, pp. 2565-2568, June 2011.
- [18] M. Barzegaran, A. Mazloomzadeh, and O. A. Mohammed, "Fault Diagnosis of the asynchronous machines through magnetic signature analysis using finite-element method and neural networks," *IEEE Trans. Energy Convers.*, vol. 28, no. 4, pp. 1064-1071, Dec 2013.
- [19] KT. Kim, YS. Lee, and J. Hur, "Transient Analysis of Irreversible Demagnetization of Permanent-Magnet Brushless DC Motor With Interturn Fault Under the Operating State," *IEEE Trans. Ind. Appl.*, vol. 50, no. 5, pp. 3357-3364, Oct 2014.
- [20] L. Romeral, J. C. Urresty, JR. R. Ruiz, and A. G. Espinosa "Modeling of Surface-Mounted Permanent magnet Synchronous Motors with Stator Winding Interturn Faults," *IEEE Trans. Ind. Electron.*, vol. 58, no. 5, pp. 1576-1585, May 2011.
- [21] J. Lee, S. Moon, H. Jeong, and S. W. Kim, "Robust Diagnosis Method Based on Parameter Estimation for an Interturn Short-Circuit Fault in Multipole PMSM under High-Speed Operation," *Sensors*, vol. 15, pp. 29452-29466, Nov 2015.
- [22] T. Sderstrom, and P. Stoica, "*System Identification*", Prentice Hall, 1989.
- [23] N. Leboeuf, T. Boileau, B. Nahid-Mobarakeh, N. Takorabet, F. Meibody-Tabar, and G. Clerc, "Inductance Calculations in Permanent-Magnet Motors Under Fault Conditions," *IEEE Trans. Magn.*, vol. 48, no. 10, pp. 2605-2616, Oct 2012.



Seokbae Moon was born in Seoul, South Korea in 1988. He received the B.S. degrees in electrical engineering from the Postech (Pohang University of Science and Technology) in 2011. He is currently working toward the Ph.D. degree with electrical engineering, Postech since 2011. His research interests are in the areas of control and system analysis with parameter estimation techniques, system analysis and fault diagnosis such as a PMSM demagnetization fault and an interturn short fault

Hyeyun Jeong was born in Jinju, South Korea in 1990. She received the B.S. in electrical engineering from Postech (Pohang University of Science and Technology) in 2014. She is currently working toward the Master degree with electrical engineering, Postech since 2014. Her research interests are in the areas of fault detection, control, and system analysis of the PMSM.

Hojin Lee was born in Yeongcheon, South Korea in 1992. He received the B.S. degrees in electrical engineering from the Postech(Pohang University of Science and Technology) in 2016. He is currently working toward the Master degree with electrical engineering, Postech since 2016. His research interests are in the areas of fault detection, control, and system analysis of the PMSM.

Sang Woo Kim (S83-M91) was born in Pyeong-taek, Korea, in 1961. He received the B.S., M.S., and Ph.D. degrees from the Department of Control and Instrumentation Engineering, Seoul National University, Seoul, Korea, in 1983, 1985, and 1990, respectively. In 1992, he joined Pohang University of Science and Technology, Pohang, Korea, as an Assistant Professor, where he is currently a Full Professor with the Department of Electrical Engineering. In 1993, he was a Visiting Fellow with the Department of Systems Engineering, Australian National University, Canberra, Australia in 1993. His current research interests are in optimal control, optimization algorithm, intelligent control, wireless communication and process automation.